Phenotypic effects of Ehlers–Danlos syndrome-associated mutation on the FnIII domain of tenascin-X

Shulin Zhuang,[1] Apichart Linhananta,[2] and Hongbin Li[1]*

[1]Department of Chemistry, University of British Columbia, Vancouver, British Columbia, Canada V6T 1Z1
[2]Department of Physics, Lakehead University, Thunder Bay, Ontario, Canada P7B 5E1

Received 5 June 2010; Revised 31 August 2010; Accepted 4 September 2010
DOI: 10.1002/pro.503
Published online 17 September 2010 proteinscience.org

Abstract: Tenascin-X (TNX) is an extracellular matrix (ECM) protein and interacts with a wide variety of molecules in the ECM as well as on the membrane. Deficiency of TNX causes a recessive form of Ehlers–Danlos syndrome (EDS) characterized by hyperelastic and fragile skin, easy bruising, and hypermobile joints. Three point mutations in TNX gene were found to be associated with hypermobility type EDS and one of such mutations is the V1195M mutation at the 7th fibronectin Type III domain (TNXfn7). To help elucidate the underlying molecular mechanism connecting this mutation to EDS, here we combined homology modeling, chemical denaturation, single molecule atomic force microscopy, and molecular dynamics (MD) simulation techniques to investigate the phenotypic effects of V1195M on TNXfn7. We found that the V1195M mutation does not alter the three-dimensional structure of TNXfn7 and had only mild destabilization effects on the thermodynamic and mechanical stability of TNXfn7. However, MD simulations revealed that the mutation V1195M significantly alters the flexibility of the C′E loop of TNXfn7. As loops play important roles in protein–protein and protein–ligand interactions, we hypothesize that the decreased loop flexibility by V1195M mutation may affect the binding of TNX to ECM molecules and thus adversely affect collagen deposition and fibrillogenesis. Our results may provide new insights in understanding the molecular basis for the pathogenesis of V1195M-resulted EDS.

Keywords: tenascin-X; Ehlers–Danlos syndrome; mutation; single-molecule force spectroscopy; molecular dynamics simulations; mechanotransduction

Introduction

Tenascin-X (TN-X) is a highly conserved glycoprotein in the extracellular matrix (ECM) and belongs to the tenascin family that consists of five members: TN-C, TN-R, TN-X, TN-Y, and TN-W.[1–4] All tenascins are tandem modular proteins and share similar domain arrangement. The constituent domains can be divided into four structurally distinct classes: an N-terminal tenascin-assembly domain involved in oligomerization, a stretch of epidermal growth factor-like repeats, a series of fibronectin Type III (FnIII) domains, and a C-terminal knob domain homologous to the globular domain of fibrinogen.[4] By interacting with a wide range of molecules in ECM and on cell membrane,[5–7] including proteins and proteoglycans, TN-X helps knit structural ECM proteins, such as collagens, with surrounding cells as well as other ECM components to form an interacting network to provide the desired mechanical strength and elasticity to connective tissues.[8] Therefore, TN-X is an important element in the mechanostranstruction process of connective tissues.[9] Such importance is further corroborated by the discovery of the direct link of deficiency and mutations in TN-X with connective tissue disorder,

Additional Supporting Information may be found in the online version of this article.

Grant sponsors: Canadian Institutes for Health Research, Michael Smith Foundation for Health Research, Canada Research Chair program, The Natural Sciences and Engineering Research Council of Canada.

*Correspondence to: Hongbin Li, Department of Chemistry, University of British Columbia, Vancouver, British Columbia, Canada V6T 1Z1. E-mail: Hongbin@chem.ubc.ca

Ehlers–Danlos Syndrome (EDS). EDS is a group of connective tissue disorders affecting skin, ligaments, joints, blood vessels, and internal organs and is typically linked to defects in genes of collagen and collagen-modifying enzymes.[10–14] A recessive form of EDS was discovered to result from deficiency and mutations in the TN-X gene.[10,13,14] Typical symptoms are hyperelastic and fragile skin, easy bruising, and hypermobile joints. Skin tissues from TN-X deficient patients show abnormal elastic fibers and reduced collagen deposition, as well as reduced mechanical strength.[8,15] TN-X is the first example of a gene outside the collagen family that causes EDS. Despite its rareness, TN-X-associated EDS reveals a new perspective for understanding the roles of TN-X in connective tissue disorder and the regulation of ECM architecture.

Recently, three point mutations in TN-X were reported to be associated with hypermobility type EDS: R29W mutation at exon 1, V1195M mutation at the seventh FnIII domain of human tenascin-X (TNXfn7), and L4033I mutation at 29th FnIII domain (TNXfn29) of human TNX. These mutations were identified in hypermobility type EDS patients and were not present in control individuals.[14] Among the three mutations, L4033I mutation does not alter the elastic fiber length in the skin of patients and is a nondeleterious mutation. In contrast, V1195M mutation occurs in a highly conserved region of TNX and causes a significant alteration of elastic fiber length in the dermis of the patients, suggesting that V1195M is likely to be disease-causing. Although it was postulated that TN-X plays indispensable roles in fibrillogenesis by specifically regulating interfibrillar distance in collagen fibrils by its interaction with collagen and decorin,[16,17] the underlying molecular mechanism for disease-causing remains unknown. Considering the role of TNX in mechanotransduction and connective tissue organization via interactions with ECM molecules, here we combine homology modeling, thermodynamic characterization, single molecule atomic force microscopy (AFM), and molecular dynamics (MD) techniques to investigate the phenotypic effects of the mutation V1195M on the structural conformation, thermodynamic and mechanical stability, as well as the flexibility and dynamics of TNXfn3.

Results

Structures of TNXfn7 and its V1195M mutant

There is a broad consensus that protein structural data is essential for characterization of biological functions at the atomic level. As the structures of TNXfn7 and its mutant V1195M have not yet been experimentally determined, we have modeled the tertiary structures of TNXfn7 and V1195M by homology modeling using I-TASSER server.[18] The I-TASSER is one of the most accurate protein structure and function prediction servers in CASP7 (Critical Assessment of Techniques for Protein Structure Prediction) and CASP8.[19]

Protein structures of the 31st FnIII domain of the human TNX (PDB ID: 2CUI), the 33rd FnIII domain of the human TNX (PDB ID: 2CUM), FnIII domain 5–6 segment from chicken tenascin (PDB ID: 1QR4), and the 2nd FnIII domain of slow type myosin-binding protein C (PDB ID: 2YUW) were chosen by I-TASSER as templates in the modeling. The predicted structure of TNXfn7 has a TM-score of 0.79 ± 0.09 and a C-score of 0.58. The modeled V1195M structure has a TM-score of 0.78 ± 0.09 and a C-score of 0.53. The TM-score measures the similarity of topologies between the modeled protein and its template, and varies from 0 to 1, where a higher value indicates strong similarity. In a study that assesses the accuracy of I-TASSER,[20] proteins with TM-score above a cutoff of 0.5 can be predicted with an average root mean square deviation (RMSD) of 2.9 Å. The *C*-score is a confidence score for estimating the quality of predicted models by I-TASSER with value typically in the range of −5 to 2, and higher values indicating predicted models of high confidence. In a recent I-TASSER assessment of a large number of proteins, *C*-scores above cutoff of 0.5, 1, and 1.5 have a prediction success rate of 94, 97, and 98%, respectively.[21] Thus, we have high confidence in the predicted structures of TNXfn7 and its V1195M mutant.

To further validate the predicted structure, the stereochemical quality of the predicted models was assessed by PROCHECK,[22] which produces Ramachandran [φ,ψ] plots (Supporting Information Figs. S1A and S2A). In the structure of TNXfn7, 97.1% of residues are in the most favorable [φ,ψ] conformations, 2.9% of residues are in the conformationally allowed regions, and no residues are in the disallowed regions. For V1195M, there are 94.3% of residues in favorable [φ,ψ] conformations, 5.7% of residues in conformationally allowed regions, and no residues in the disallowed regions. This assessment clearly showed the high quality of the predicted models. We further evaluate the models with Prosa web server,[23] which gives the *Z*-score of −6.59 and −6.71 for the predicted structures of TNXfn7 and V1195M, respectively. The *Z*-scores of the predicted TNXfn7 and V1195M structures are within the range of *Z*-scores of X-ray- and NMR-resolved native structures of proteins of similar size (Supporting Information Figs. S1B and S2B), indicating the high quality of the predicted models.

The predicted native structures of TNXfn7 and its mutant V1195M (Fig. 1) show β-sandwich structures, which are typical of immunoglobulin(Ig)-like domains, such as fibronectin Type III domains of known structures from TN-C.[24] The two β-sheets are packed against each other with the top A-B-E

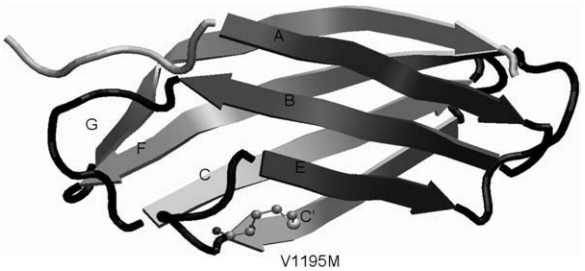

Figure 1. The tertiary structure of V1195M by homology modeling. TNXfn7 has a typical Ig-like β-sandwich structure with the top β-sheet (consisting of A-B-E strands colored in black) packing against the bottom C′-C-F-G β-sheet (colored in gray). The seven β strands are connected by six loops (dark color). Mutation V1195M is highlighted by ball-and-stick representation.

β-sheet (black) aligned 30° counterclockwise with respect to the bottom C′-C-F-G β-sheet (gray). The seven β strands are connected by six loops (dark). The V1195M mutation occurs at the end of C′E loop, and is highlighted by the ball-and-stick representation (Fig. 1). The superimposition of the two structures of TNXfn7 and V1195M indicate that these two domains show nearly identical topologies. The calculated Cα RMSD between wild type TNXfn7 and its mutant V1195M is 0.25 Å, indicative of virtually no change in coarse-grain structure caused by V1195M mutation.

To experimentally verify that the mutation V1195M does not alter the overall three-dimensional structure of TNXfn7, we carried out far ultraviolet (UV) circular dichroism spectroscopy experiments. As shown in Figure 2, the CD spectrum of wt TNXfn7 shows a minimum at ~215 nm, indicative of a β-sheet-like secondary structure, which is consistent with the homology prediction. The CD spectrum

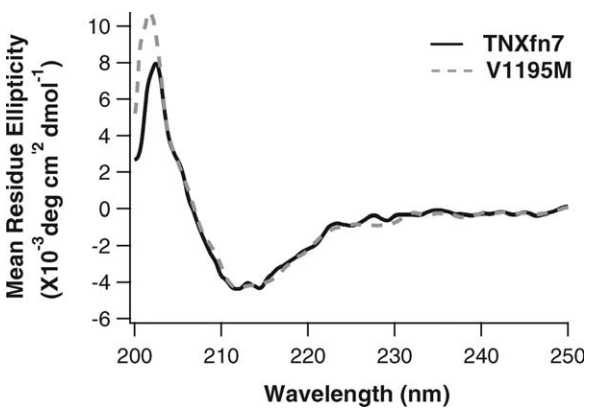

Figure 2. Far-UV CD spectra of TNXfn7 and its mutant V1195M. The CD spectra of TNXfn7 (in black) and V1195M (in gray) are typical of β-sheet proteins, confirming that TNXfn7 and its V1195M are well folded. The CD spectra of wt TNXfn7 and mutant V1195M are almost identical, indicating mutation V1195M does not result in significant structural changes of TNXfn7.

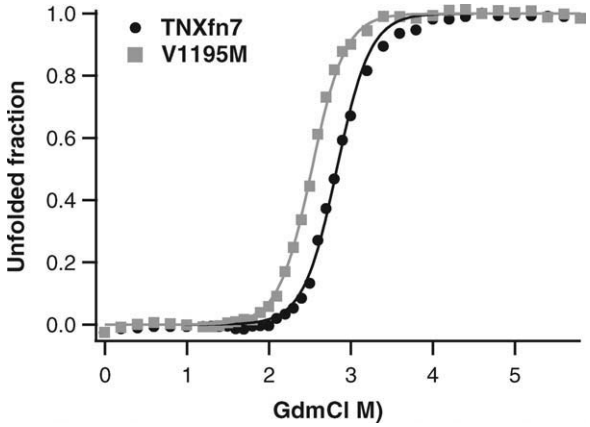

Figure 3. Equilibrium denaturation curves for TNXfn7 (circle) and V1195M (square). The denaturation curve of V1195M shifts toward slightly lower [GdmCl] as compared with that of wt TNXfn7, suggesting that mutation V1195M destabilizes TNXfn7. Fitting the equilibrium unfolding curves (solid lines) with a two-state model measured a decrease of thermodynamic stability of TNXfn7 by ~0.8 kcal/mol.

of V1195M is almost identical to that of wt TNXfn7, suggesting that the mutation V1195M does not cause major change to the secondary structure of TNXfn7, consistent with the prediction of homology modeling.

Mutation V1195M leads to a slight decrease in thermodynamic stability of TNXfn7

Thermodynamic stability of proteins determines the state of proteins in their biologically relevant environment, and individual mutations may significantly affect the thermodynamic stability of proteins. To investigate the possible effect of the V1195M mutation on the thermodynamic stability of TNXfn7, we used chemical denaturation to directly evaluate the effect of V1195M on the thermodynamic stability of TNXfn7 by using tryptophan fluorescence as a probe. The equilibrium denaturation curves (Fig. 3) indicate that both wt and V1195M mutant unfold in an apparent two-state fashion, and the thermodynamic stability of both proteins can be determined from $[GdmCl]_{0.5}$, at which 50% of the protein is unfolded. It is evident that $[GdmCl]_{0.5}$ for V1195M shifted slightly toward lower value as compared with that of wt TNXfn7 (2.52 *M* for V1195M vs. 2.83 *M* for wt), suggesting that the mutation V1195M resulted in slight destabilization of TNXfn7. Fitting the equilibrium unfolding curves with a two-state model revealed that mutation V1195M resulted in a decrease in thermodynamic stability of TNXfn7 by ~0.8 kcal/mol.

Mutation V1195M has a mild effect on the mechanical stability of TNXfn7

TN-X is an important element in the mechanotransduction network of connective tissues and is subject

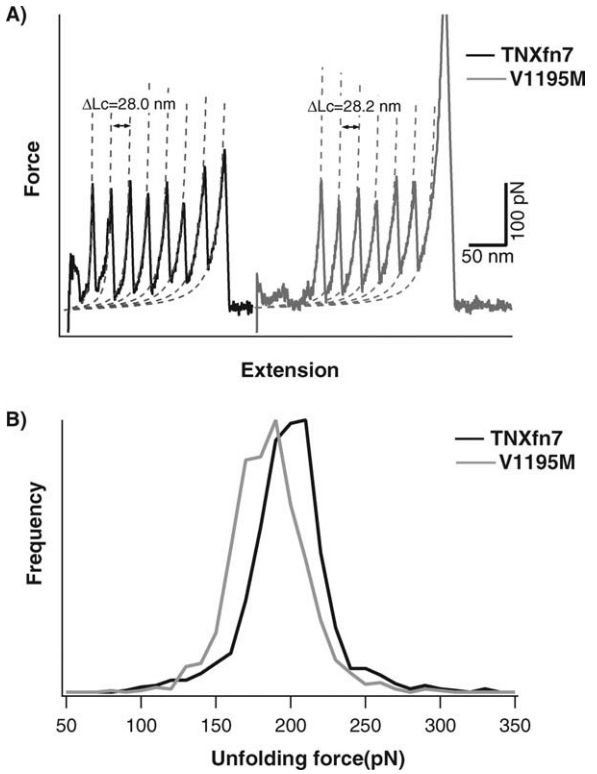

Figure 4. Mutation V1195M leads to a slight decrease in the mechanical stability of TNXfn7. A) Typical force-extension curves of $(TNXfn7)_8$ (in black) and $(V1195M)_8$ (in gray). Dotted lines correspond to the WLC fits. The mechanical unfolding of mutant V1195M and wt TNXfn7 show virtually identical contour length increment ΔL_c of ~28 nm. B) Unfolding force histograms for TNXfn7 (in black) and V1195M (in gray). The average unfolding force is 204 ± 29 pN (avg. ± S.D., $n = 866$) for wt TNXfn7 and is 190 ± 25 pN ($n = 923$) for V1195M.

to stretching force under its physiological conditions. The nanomechanical properties of bovine TN-X have been characterized in detail using single molecule AFM techniques.[25] To investigate the mechanical phenotypical effect of mutation V1195M on the mechanical stability of TN-X, we used single molecule AFM[26,27] to directly measure the mechanical stability of wt and mutant TNXfn7. To facilitate the characterization of the mechanical stability of TNXfn7, we used the well-developed polyprotein engineering approach[28] to construct polyproteins $(TNXfn7)_8$ and $(V1195M)_8$, which consist of eight identical tandem repeat of either TNXfn7 or V1195M.

Stretching the polyprotein $(TNXfn7)_8$ results in force-extension curves showing characteristic sawtooth pattern appearance, in which the equally spaced sawtooth peaks correspond to the sequential mechanical unfolding of individual TNXfn7 domains (Fig. 4A). The last peak corresponds to the stretching and subsequent detachment of the unfolded polyprotein chain from either the AFM tip or substrate. The amplitude of this detachment peak, ranging from a few hundred pN to more than 1 n*N*, reflects the adhesion force between TNXfn7 and the glass substrate (or the tip) and thus has nothing to do with the unfolding of TNXfn7 domains. Fitting the worm-like-chain (WLC) model of polymer elasticity[29] (dashed line) to the consecutive unfolding force peaks measured a contour length increment ΔL_c of ~28 nm for TNXfn7, in good agreement with the contour length increment of TNXfn domains measured previously.[25] The mechanical unfolding of TNXfn7 occurs at an average force of 204 ± 29 pN ($n = 866$) at a pulling speed of 400 nm/s (Fig. 4B), which is much higher than the average unfolding force of bovine TNXfn domains (148 ± 26 pN)[25] and FnIII domains from TN-C.[26,30,31] This difference in mechanical stability among homologous protein domains has been observed in different proteins, such as titin Ig domains[32] and fibronectin FnIII domains,[33] and should have its origin in the atomic structures of proteins. However, because of the lack of complete understanding of molecular determinants of mechanical stability of proteins, it is not possible to account for the difference in mechanical stability of different FnIII domains from their structures.

In comparison with wt TNXfn7, the mechanical unfolding of the mutant V1195M did not show any major difference. The measured contour length increment ΔL_c of V1195M is virtually identical to that of wt TNXfn7. The mechanical unfolding force of V1195M is 190 ± 25 pN ($n = 923$), which is slightly lower than that of wt TNXfn7. From the unfolding force histogram and the pulling speed dependence of unfolding forces (data not shown), we used well-established Monte Carlo method[28] to measure the mechanical unfolding rate constant at zero force α_0, which in turn allowed us to calculate the change of the unfolding energy barrier $\Delta\Delta G_{T\text{-}N}$ due to mutation using the following relationship: $\Delta\Delta G_{T-N} = -RTln(\alpha_0^{mut}/\alpha_0^{wt})$, where R is the gas constant, T is temperature, and α_0^{mut} and α_0^{wt} are unfolding rate constant of mutant and wild-type protein, respectively. A change of the unfolding energy barrier due to mutation was calculated to be ~0.8 kcal/mol. The amplitude of this destabilization effect is similar to that of thermodynamic destabilization. However, because of the difference in the kinetic stability (ΔG_{N_T}) versus thermodynamic stability ($\Delta G_{N\text{-}U}$), the nearly identical value of $\Delta\Delta G_{N\_T}$ and $\Delta\Delta G_{N\_U}$ may be coincidental, and no conclusion can be directly made on the effect of the mutation on the stability of the native and unfolded state.

Dynamics and flexibility investigation of V1195M mutation

TNX interacts with a variety of molecules in ECM as well as on the cell membrane.[5–7,15] However, most binding epitopes of TNX have not been mapped out. It is possible that TNXfn7 may interact with ECM molecules and play important roles in the

organization of connective tissues. For this purpose, we used MD simulations to investigate the effect of the mutation of V1195M on the flexibility of TNXfn7.

It is now widely recognized that protein flexibility plays key roles in protein functions, such as enzyme catalysis, allosteric regulation, and binding. For example, NMR and fluorescence studies have detected correlation between movements at specific sites and protein functions of calmodulin, T4 lysozyme, and troponin C.[34] Measurement of flexibility is usually challenging for experiments, making theoretical methods and MD an important tool in characterizing how the flexibility of proteins regulates functions. Pikkemaat *et al*.[35] performed 1.2 ns MD simulations (with GROMOS) to identify flexible regions of Haloakane dehalogenase (DhlA) and its mutants. Verma and Fischer[36] used normal mode analysis on bovine pancreatic trypsin inhibitor (BPTI) and its Gly36Ser mutant, and found reduced fluctuations and flexibility in the mutant compare with the wild type. In a recent work, Arcangeli *et al*.[37] used homology modeling and 15.5 ns MD simulations (with AMBER) to assess the stability and dynamics of mutants of anti-AMVC scFv(F8). In the same spirit as these works, we performed large-scale MD simulations to investigate the effects of the V1195M mutation on the dynamics and flexibility of TNXfn7.

Nanoseconds MD simulations are not sufficient for complete thermodynamics evaluation of proteins, but are usually sufficient for reliable assessments of local conformational changes. Here, we performed two 47 ns all-atom MD simulations using AMBER on TNXfn7 and V1195M mutant in explicit solvent at 300 K in isothermal isobaric (NPT) ensemble. We calculated the instantaneous Cα RMSD of TNXfn7 and V1195M mutant along the 47 ns MD trajectories by using the predicted structures as references. As shown in the RMSD-time plots [Fig. 5(A)], both trajectories fluctuate uniformly about RMSD values of 2 Å. The average Cα RMSD of TNXfn7 and V1195M is 1.89 and 1.66 Å, respectively. In all-atom MD simulation studies, a uniform RMSD distribution of about 2 Å is generally regarded as stable protein structures.[37] This is an additional validation of the predicted structures of TNXfn7 and V1195M obtained with I-TASSER. The Cα RMSD analysis of individual subunits of TNXfn7 and V1195M shows that most of the subunits are comparatively rigid. The structural fluctuations of TNXfn7 arise mainly from BC loop (average Cα RMSD:1.23 Å) and C′E loop(average Cα RMSD:1.37 Å). However, for V1195M mutant, the main structural fluctuation arises only from BC loop (average Cα RMSD:1.65 Å). The average Cα RMSD of C′E loop in V1195M is only 0.51 Å. Compared with C′E loop of TNXfn7, the V1195M mutant has a much lower Cα RMSD for C′E loop, showing a reduced amplitude of motion in the C′E loop. These results suggest that mutation V1195M significantly reduced the flexibility of TNXfn7.

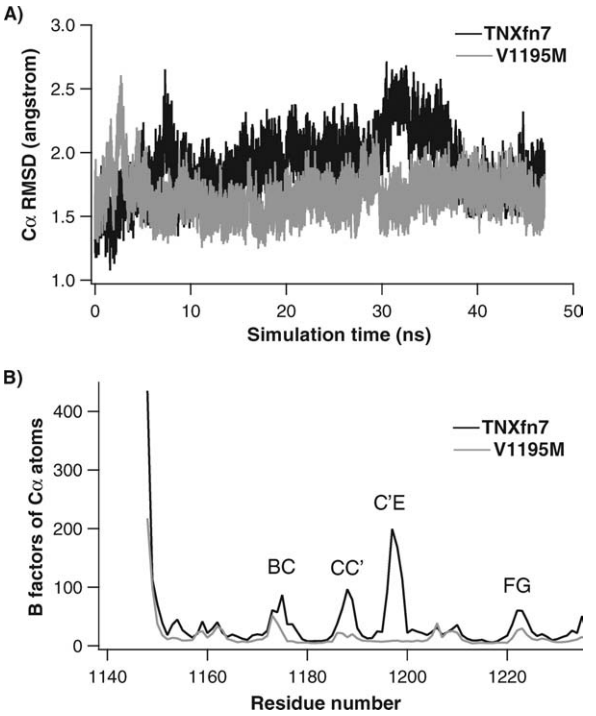

Figure 5. The RMSD and B-factors distribution of Cα atoms. (A) The Cα RMSD calculated from 47 ns MD trajectories. Using the minimized structure as the reference, the average Cα RMSD calculated for TNXfn7 and V1195M is 1.89 and 1.66 Å, respectively. The overall trend of the Cα RMSD distribution differs slightly between TNXfn7 and V1195M. (B) The calculated B-factors distribution of Cα atoms from the last 42 ns MD trajectories. The B-factors of Cα atoms reflect the remarkable difference between the loop flexibility of TNXfn7 (in black) and V1195M (in gray). Compared with TNXfn7, V1195M has a lower B-factor ordered regions in loops BC, CC′, C′E, and FG, indicating a significantly reduced flexibility caused by the V1195M mutation.

Crystallographically determined B-factor measures the fluctuations of atoms about their average positions, and are commonly used to evaluate the residue-level flexibility of folded proteins.[38,39] B-factors can also be estimated by computational approaches such as the MD simulations.[40] Here, we calculated the B-factor of TNXfn7 and V1195M from the last 42 ns MD trajectories (the first 5 ns were omitted to allow for equilibration) of both proteins and the results are shown in Figure 5(B). It is striking that the plots reveal that the atomic flexibility of wt TNXfn7 (dark color) is much greater than that of the V1195M mutant (gray color). TNXfn7 has five high B-factor regions, the N-termini, BC loop, CC′ loop, C′E loop, and FG loop. In contrast, V1195M shows lower B-factor in regions of the BC loop, CC′ loop, C′E loop, and FG loop. The contrast in flexibility is especially evident for the C′E loop. Taken together, our MD

simulation results show that the V1195M mutation dramatically reduced the flexibility of TNXfn7.

It is possible that the reduced flexibility of V1195M is due to the change from a β-branched (valine) to non-β-branched (methionine) residue. To test this hypothesis, we performed simulations on V1195I, a β-branched to β-branched mutation, and V1195A, a β-branched to non-β-branched mutation. Homology modeling and MD simulations were performed on these mutants following the same protocol as for TNXfn7 and V1195M. The result of all B-factor analysis is shown in Supporting Information Figure S3. Comparison of the wild-type TNXfn7 (black) with the β-branched to non-β-branched mutants, V1195M (gray) and V1195A (red), clearly show a significant overall decrease in flexibility of the mutants, especially at the BC loop, CC′ loop, and CE′ loop. The exception is the FG loop, where there is a slight increase in the flexibility of the V1195A mutant. In contrast, the β-branched to β-branched V1195I mutant (blue) shows similar flexibility as TNXfn7, with similar B-factor at BC loop, C′E loop, and FG loop, but with reduced B-factor at CC′ loop. Taking all the MD results together, we conclude that the reduced flexibility of V1195M compared with the wild type is likely due to the change from a β-branched to a non-β-branched residue at site 1195.

Discussion

Using a combination of experimental and computational methods, we have investigated the effect of the EDS-associated V1195M mutation on the structural conformation, mechanical stability, thermodynamic stability, as well as protein dynamics and flexibility of human TNXfn7 in detail.

We found that the mutation V1195M does not alter the three-dimensional structure of TNXfn7 and has only small destabilizing effects on the thermodynamic and mechanical stability of TNXfn7. These results are not surprising, as the mutation V1195M is located at the beginning of a solvent-exposed C′E loop and the mutation V1195M does not involve dramatic change of the characteristics of the amino acid residue. These relatively mild thermodynamic and mechanical destabilization effects suggest that thermodynamic and mechanical reasons are unlikely to be the major cause of pathogenesis of hypermobility type EDS.

The most pronounced phenotypic effect for the mutation V1195M is the change of the flexibility of TNXfn7. The Cα RMSD analysis showed that the amplitude of motion in the C′E loop of TNXfn7 is greatly reduced by the mutation V1195M. The loops of TNXfn7 and V1195M exhibit extensive flexibility from picosecond to nanosecond timescales, a behavior similar to that of loops of FNfn10 and TNfn3 domains.[41] The BC loop, CC′ loop, C′E loop, and FG loop of TNXfn7 constitute a high B-factor region, showing the flexible features of the loops. In contrast, the B-factors of V1195M Cα atoms in the same regions are remarkably lower, suggesting that the mutation V1195M dramatically reduced the loop flexibility.

A paradoxical result is that MD simulations found reduced flexibility in the native structure of V1195M, but chemical denaturation data show a slight decrease in thermodynamic stability. This is intuitively puzzling as various studies suggest that protein stability is inversely correlated with protein flexibility.[42] However, previous studies also reported cases where an increase in protein flexibility is correlated with an increase in thermal stability.[43] The fact that MD simulations (Fig. 5) found the folded state of V1195M to be less flexible than that of TNXfn7 does suggest that the folded state of the V1195M is more stable, but this does not mean that V1195M has greater thermodynamic stability. The overall thermodynamic stability of V1195M depends on the stability of its folded and unfolded states. The decrease in flexibility and in thermodynamic stability of V1195M suggests that the mutation stabilizes the unfolded state. Unfortunately, current computational powers are still not sufficient for a direct MD assessment of the thermodynamic stability of TNXfn7 and V1195M.

Protein flexibility is of fundamental importance to its biological functionality, and there is an increasing awareness of the importance of intrinsic disorder and flexibility to protein function.[44] The change of protein flexibility may affect its ability to adapt its structural conformation upon the binding of its ligand. For TNXfn7, the V1195M mutation results in a dramatically reduced flexibility for C′E loop, which can dynamically interacts with BC loop, FG loop. Consequently, the reduced flexibility of the C′E loop affects the flexibility of BC loop, FG loop, and CC′ loop, leading to the overall decreased flexibility of these loops. Their combined effects may affect the ability of TNXfn7 to bind to its ligands. As TNX is an important regulator of the deposition of collagen fibrils in the ECM[14] via its binding to glycosaminoglycan chains of the small fibril-associated proteoglycans,[16,45] we hypothesize that TNXfn7 is a potential binding site for molecules that are involved in collagen deposition. Dramatically reduced flexibility in the mutant V1195M may alter the binding properties of TNXfn7 to such molecules and thus affect the normal deposition of collagen fibrils. Hence, our results may open up a new avenue to illustrate the molecular origin of the pathogenesis of V1195M-related hypermobility type EDS, and provide new insights into the role of TNX in the organization and function of connective tissues.

Material and Methods

Protein engineering

The amino acid sequence of TNXfn7, obtained from NCBI(TNXB isoform 1 precursor of Homo sapiens,

GI: 188528648), is 88 residues long (GPPRLGELTVT DRTSDSLLL RWTVPEGEFDSFVIQYKDRDGQPQV VP**V**EGPQRSAVITSLDPGRKYKFVLYGFVGKKRHG PLVAEAKI, where the highlighted residue V corresponds to the reported V1195 residue that is affected by mutation V1195M). This sequence was used for homology modeling. In protein engineering work, we included four additional residues from its natural neighboring FnIII domains at the N- and C-termini of TNXfn7 (SS at the N-terminus and LP at the C-terminus, respectively). The gene encoding this extended version of TNXfn7 (Supporting Information) was synthesized by Genscript company (http://www.genscript.com/) and its codon-usage was optimized using the Genscript's software. Using wt TNXfn7 as the template, the mutant V1195M was obtained by using standard site-directed mutagenesis techniques, and the sequence was verified by direct DNA sequencing. The polyprotein genes $(TNXfn7)_8$ and $(V1195M)_8$ was constructed using a previously described step-by-step procedures[46] based on the identity of the sticky ends generated by digesting BamHI and BglII sites. The polyproteins were expressed in *E. coli* DH5α strain at 37°C following standard protocols. The polyproteins were purified by Ni^{2+} affinity chromatography and eluted in PBS buffer containing 300 m*M* NaCl and 250 m*M* imidazole. Imidazole was removed by dialysis against PBS buffer (pH 7.4) at 4°C.

Circular dichroism spectroscopy

The far-UV CD spectroscopy was performed on a Jasco-J810 spectropolarimeter at room temperature. The data was collected from 200 to 250 nm with a pathlength of 2 cm at a scan speed of 50 nm/min. The average of three scans was reported. The CD intensities was calculated as mean residue ellipticity with reported protocols.[47]

Fluorescence spectroscopy

The GdmCl-induced denaturation experiments were performed on a Cary Eclipse Fluorescence Spectrophotometer using tryptophan fluorescence as a probe. The excitation wavelength and emission wavelength were set at 280 nm and 370 nm, respectively. To measure the thermodynamics stability of proteins, the equilibrium denaturation curves were fitted using the two-state model,[48] and the thermodynamic stability was calculated as $\Delta G = m[GdmCl]_{0.5}$.

Single-molecule force spectroscopy

All the single-molecule force spectroscopy experiments were performed with a custom-built atomic force microscope as described previously[46,49] in Tris-HCl buffer (10 m*M*, pH 7.4, containing 100 m*M* NaCl) at room temperature. Before each AFM measurement, the AFM Si3N4 cantilever (Veeco, Santa Barbara, CA) was calibrated using the equipartition theorem. The Igor Pro software was used for data collection and analysis.

Homology modeling

The three-dimensional structures of TNXfn7 and V1195M mutant were modeled by I-TASSER server (http://zhang.bioinformatics.ku.edu/I-TASSER/) based on multiple-threading alignments by LOMETS and iterative TASSER simulations.[18] The overall quality of the generated models was evaluated by Procheck program[22] and Prosa web server (http://prosa.services.came.sbg.ac.at/prosa.php).[23]

MD simulations

Large scale MD simulations were performed by Sander module of AMBER 10 simulation package with ff03 force field.[50] The modeled proteins were solvated in a periodic rectangular parallelepiped solvent box with 15 Å TIP3P waters and finally neutralized with Cl- ions using SLEAP module of AMBER 10 simulation package. The resultant systems have a dimension of ~65 Å × 60 Å × 75 Å with 25214, 29280 atoms in total for TNXfn7, V1195M, respectively.

The long-range electrostatic interactions were treated with the particle mesh Ewald method.[51] The nonbonded cutoff was set at 12 Å. All hydrogen-heavy atom bond lengths were constrained by Shake algorithm.[52] A time step of 2 fs was used for minimization and MD simulations. For energy minimization, 1500 cycles of steepest descent minimization followed by 1000 cycles of conjugated gradient minimization was carried out. The minimized systems were heated from 0 to 300 K at constant volume in 20 ps. The systems were subsequently equilibrated for 47 ns at 300 K in NPT ensemble. The analysis of MD trajectories was performed with PTRAJ module of AMBER 10 simulation package and structures were visualized using the VMD program.[53]

Acknowledgments

This work is supported by Canadian Institutes for Health Research Operating Grant MOP-81225, Michael Smith Foundation for Health Research and Canada Research Chairs Program. H. L. is a Michael Smith Foundation for Health Research Career Investigator. The simulation part of this work was made possible by the facilities of the Shared Hierarchical Academic Research Computing Network of Canada (SHARCNET:www.sharcnet.ca).

References

1. Chiquet-Ehrismann R (1995) Tenascins, a growing family of extracellular matrix proteins. Experientia 51: 853–862.
2. Elefteriou F, Exposito JY, Garrone R, Lethias C (1997) Characterization of the bovine tenascin-X. J Biol Chem 272:22866–22874.
3. Erickson HP (1993) Tenascin-C, tenascin-R and tenascin-X: a family of talented proteins in search of functions. Curr Opin Cell Biol 5:869–876.
4. Jones FS, Jones PL (2000) The tenascin family of ECM glycoproteins: structure, function, and regulation during embryonic development and tissue remodeling. Dev Dyn 218:235–259.

5. Elefteriou F, Exposito JY, Garrone R, Lethias C (2001) Binding of tenascin-X to decorin. FEBS Lett 495: 44–47.
6. Elefteriou F, Exposito JY, Garrone R, Lethias C (1999) Cell adhesion to tenascin-X mapping of cell adhesion sites and identification of integrin receptors. Eur J Biochem 263:840–848.
7. Chiquet-Ehrismann R, Chiquet M (2003) Tenascins: regulation and putative functions during pathological stress. J Pathol 200:488–499.
8. Egging D, van Vlijmen-Willems I, van Tongeren T, Schalkwijk J, Peeters A (2007) Wound healing in tenascin-X deficient mice suggests that tenascin-x is involved in matrix maturation rather than matrix deposition. Connect Tissue Res 48:93–98.
9. Vogel V (2006) Mechanotransduction involving multimodular proteins: converting force into biochemical signals. Annu Rev Biophys Biomol Struct 35: 459–488.
10. Burch GH, Gong Y, Liu W, Dettman RW, Curry CJ, Smith L, Miller WL, Bristow J (1997) Tenascin-X deficiency is associated with Ehlers–Danlos syndrome. Nat Genet 17:104–108.
11. Mao JR, Taylor G, Dean WB, Wagner DR, Afzal V, Lotz JC, Rubin EM, Bristow J (2002) Tenascin-X deficiency mimics Ehlers–Danlos syndrome in mice through alteration of collagen deposition. Nat Genet 30:421–425.
12. Uitto J, Ringpfeil F (2004) Ehlers–Danlos syndrome-molecular genetics beyond the collagens. J Invest Dermatol 122:xii–xiii.
13. Zweers MC, van Vlijmen-Willems IM, van Kuppevelt TH, Mecham RP, Steijlen PM, Bristow J, Schalkwijk J (2004) Deficiency of tenascin-X causes abnormalities in dermal elastic fiber morphology. J Invest Dermatol 122:885–891.
14. Zweers MC, Dean WB, van Kuppevelt TH, Bristow J, Schalkwijk J (2005) Elastic fiber abnormalities in hypermobility type Ehlers–Danlos syndrome patients with tenascin-X mutations. Clin Genet 67:330–334.
15. Egging D, van den Berkmortel F, Taylor G, Bristow J, Schalkwijk J (2007) Interactions of human tenascin-X domains with dermal extracellular matrix molecules. Arch Dermatol Res 298:389–396.
16. Bristow J, Carey W, Egging D, Schalkwijk J (2005) Tenascin-X, collagen, elastin, and the Ehlers–Danlos syndrome. Am J Med Genet C Semin Med Genet 139: 24–30.
17. Minamitani T, Ikuta T, Saito Y, Takebe G, Sato M, Sawa H, Nishimura T, Nakamura F, Takahashi K, Ariga H, Matsumoto K (2004) Modulation of collagen fibrillogenesis by tenascin-X and type VI collagen. Exp Cell Res 298:305–315.
18. Zhang Y (2008) I-TASSER server for protein 3D structure prediction. BMC Bioinformatics 9:40.
19. Zhang Y (2009) I-TASSER: fully automated protein structure prediction in CASP8. Proteins 77:100–113.
20. Zhang Y, Skolnick J (2005) TM-align: a protein structure alignment algorithm based on the TM-score. Nucleic Acids Res 33:2302–2309.
21. Zhang Y, Devries ME, Skolnick J (2006) Structure modeling of all identified G protein-coupled receptors in the human genome. PLoS Comput Biol 2:e13.
22. Laskowski RA, MacArthur DS, Thornton JM (1993) PROCHECK: a program to check the stereochemical quality of protein structures. J Appl Cryst 26:283–291.
23. Wiederstein M, Sippl MJ (2007) ProSA-web: interactive web service for the recognition of errors in three-dimensional structures of proteins. Nucleic Acids Res 35:W407–W410.
24. Leahy DJ, Hendrickson WA, Aukhil I, Erickson HP (1992) Structure of a fibronectin type III domain from tenascin phased by MAD analysis of the selenomethionyl protein. Science 258:987–991.
25. Jollymore A, Lethias C, Peng Q, Cao Y, Li H (2009) Nanomechanical properties of Tenascin-X revealed by single-molecule force spectroscopy. J Mol Biol 385: 1277–1286.
26. Oberhauser AF, Marszalek PE, Erickson HP, Fernandez JM (1998) The molecular elasticity of the extracellular matrix protein tenascin. Nature 393:181–185.
27. Rief M, Gautel M, Oesterhelt F, Fernandez JM, Gaub HE (1997) Reversible unfolding of individual titin immunoglobulin domains by AFM. Science 276: 1109–1112.
28. Carrion-Vazquez M, Oberhauser AF, Fowler SB, Marszalek PE, Broedel SE, Clarke J, Fernandez JM (1999) Mechanical and chemical unfolding of a single protein: a comparison. Proc Natl Acad Sci USA 96: 3694–3699.
29. Marko JF, Siggia ED (1995) Stretching DNA. Macromolecules 28:8759–8770.
30. Peng Q, Zhuang S, Wang M, Cao Y, Khor Y, Li H (2009) Mechanical design of the third FnIII domain of tenascin-C. J Mol Biol 386:1327–1342.
31. Ng SP, Rounsevell RW, Steward A, Geierhaas CD, Williams PM, Paci E, Clarke J (2005) Mechanical unfolding of TNfn3: the unfolding pathway of a fnIII domain probed by protein engineering, AFM and MD simulation. J Mol Biol 350:776–789.
32. Li H, Linke WA, Oberhauser AF, Carrion-Vazquez M, Kerkvliet JG, Lu H, Marszalek PE, Fernandez JM (2002) Reverse engineering of the giant muscle protein titin. Nature 418:998–1002.
33. Oberhauser AF, Badilla-Fernandez C, Carrion-Vazquez M, Fernandez JM (2002) The mechanical hierarchies of fibronectin observed with single-molecule AFM. J Mol Biol 319:433–447.
34. Gerstein M, Krebs W (1998) A database of macromolecular motions. Nucleic Acids Res 26:4280–4290.
35. Pikkemaat MG, Linssen AB, Berendsen HJ, Janssen DB (2002) Molecular dynamics simulations as a tool for improving protein stability. Protein Eng 15:185–192.
36. Verma CS, Fischer S (2005) Protein stability and ligand binding: new paradigms from in-silico experiments. Biophys Chem 115:295–302.
37. Arcangeli C, Cantale C, Galeffi P, Rosato V (2008) Structure and dynamics of the anti-AMCV scFv(F8): effects of selected mutations on the antigen combining site. J Struct Biol 164:119–133.
38. Ringe D, Petsko GA (1986) Study of protein dynamics by X-ray diffraction. Meth Enzymol 131:389–433.
39. Parthasarathy S, Murthy MR (2000) Protein thermal stability: insights from atomic displacement parameters (B values). Protein Eng 13:9–13.
40. Karplus M, McCammon JA (2002) Molecular dynamics simulations of biomolecules. Nat Struct Biol 9:646–652.
41. Carr PA, Erickson HP, Palmer AG, III (1997) Backbone dynamics of homologous fibronectin type III cell adhesion domains from fibronectin and tenascin. Structure 5:949–959.
42. Tang KE, Dill KA (1998) Native protein fluctuations: the conformational-motion temperature and the inverse correlation of protein flexibility with protein stability. J Biomol Struct Dyn 16:397–411.
43. Gabellieri E, Balestreri E, Galli A, Cioni P (2008) Cavity-creating mutations in Pseudomonas aeruginosa azurin: effects on protein dynamics and stability. Biophys J 95:771–781.

44. Predrag R, Zoran O, David KS, Guang Z, Slobodan V, Celeste JB, Lawson JD, Dunker AK (2004) Protein flexibility and intrinsic disorder. Protein Sci 13:71–80.
45. Veit G, Hansen U, Keene DR, Bruckner P, Chiquet-Ehrismann R, Chiquet M, Koch M (2006) Collagen XII interacts with avian tenascin-X through its NC3 domain. J Biol Chem 281:27461–27470.
46. Cao Y, Yoo T, Li H (2008) Single molecule force spectroscopy reveals engineered metal chelation is a general approach to enhance mechanical stability of proteins. Proc Natl Acad Sci USA 105:11152–11157.
47. Sharma D, Cao Y, Li H (2006) Engineering proteins with novel mechanical properties by recombination of protein fragments. Angew Chem Int Ed Engl 45:5633–5638.
48. Fersht AR (1999) Structure and Mechanism in Protein Science. W H Freeman & Co, New York.
49. Cao Y, Li H (2006) Single molecule force spectroscopy reveals a weakly populated microstate of the FnIII domains of tenascin. J Mol Biol 361:372–381.
50. Case DA, Darden TA, Cheatham TE III, Simmerling CL, Wang J, Duke RE, Luo R, Crowley M, Walker RC, Zhang W, Merz KM, Roberts BP, Wang B, Hayik S, Roitberg A, Seabra G, Kolossvary I, Wong KF, Paesani F, Vanicek J, Wu X, Brozell SR, Steinbrecher T, Gohlke H, Cai Q, Ye X, Wang J, Hsieh MJ, Cui G, Roe DR, Mathews DH, Seetin MG, Sagui C, Babin V, Luchko T, Gusarov S, Kovalenko A, Kollman PA (2008) AMBER 10, University of California: San Francisco.
51. Darden T, York D, Pedersen L (1993) Particle mesh Ewald: an N-log(N) method for Ewald sums in large systems. J Chem Phys 98:10089–10092.
52. Ryckaert J, Ciccotti G, Berendsen H (1977) Numerical integration of the cartesian equations of motion of a system with constraints: molecular dynamics of n-alkanes. J Comput Phys 23:327–341.
53. Humphrey W, Dalke A, Schulten K (1996) VMD: visual molecular dynamics. J Mol Graph 14:33–38, 27–28.